Journal of Solid Mechanics Vol. 12, No. 2 (2020) pp. 438-454
DOI: 10.22034/jsm.2019.1871279.1459

In-Plane Analysis of an FGP Plane Weakened by Multiple Moving Cracks

R. Bagheri [1,*], M. Mahmoudi Monfared [2]

[1]*Department of Mechanical Engineering, Karaj Branch, Islamic Azad University, Karaj, Iran*
[2]*Department of Mechanical Engineering, Hashtgerd Branch, Islamic Azad University, Hashtgerd, Iran*

Received 19 March 2020; accepted 14 May 2020

ABSTRACT

In this paper, the analytical solution of an electric and Volterra edge dislocation in a functionally graded piezoelectric (FGP) medium is obtained by means of complex Fourier transform. The system is subjected to in-plane mechanical and electrical loading. The material properties of the medium vary exponentially with coordinating parallel to the crack. In this study, the rate of the gradual change of the shear moduli and mass density is assumed to be same. At first, the Volterra edge dislocation solutions are employed to derive singular integral equations in the form of Cauchy singularity for an FGP plane containing multiple horizontal moving cracks. Then, these equations are solved numerically to obtain dislocation density functions on moving crack surfaces. Finally, the effects of the crack moving velocity, material properties, electromechanical coupling factor and cracks arrangement on the normalized mode I and mode II stress intensity factors and electric displacement intensity factor are studied.

Keywords: Mixed mode loading; Multiple moving cracks; Functionally graded piezoelectric materials; Dislocation technique; Field intensity factors.

1 INTRODUCTION

PIEZOELECTRIC materials have been extensively used in electromechanical devices. These kinds of devices have played a significant role in the smart systems of aerospace, automotive, medical and electronic fields [1]. Mechanically and electrically induced stresses can cause premature failure of these devices due to the propagation of flaws or defects during production and/or in-service condition. Functionally graded materials (FGMs) play an important role in many complex systems for their superior properties. In most cases, FGMs are inhomogeneous with properties varying spatially and characterized by gradually changing material constants. In order to improve their application and reliability, FGMs can be extended to piezoelectric materials. When FGM

*Corresponding author. Tel: +98 263 4182442.
E-mail address: r.bagheri@kiau.ac.ir (R. Bagheri).

materials are combined with piezoelectric properties, new materials emerge known as functionally graded piezoelectric materials (FGPMs). These materials are widely used because of both of these properties and are used in important fields such as aerospace, nuclear power, chemical plants, electronics and biomaterials. On the other hand, since FGPM materials have a doping effect between the elastic domain and the electric domain, they are therefore widely used in the manufacture of actuators or sensors in intelligent composite systems. The physical properties of FGPMs are non-homogeneous and the electro- mechanical parameters may vary continuously in particular directions. The main advantage of FGPMs over conventional composites is the absence of any interfaces. It is generally well known that FGPMs are very brittle and capable to fracture with low toughness. Thus, the investigation of the fracture analyses of piezoelectric materials could provide information to improve the design of electromechanical devices. For the cracks in piezoelectric solids and stress analysis in cracked materials, one of the most important issues is to investigate the fracture parameters, such as microstructural parameters, stress intensity factors and *J*-integral by employing the advanced numerical method [2–4]. Clearly, a moving crack has completely different characteristics from the static one. Great progress has been made in the analysis of cracks in bodies made up of FGMs. A brief review of the articles regarding the crack problem in piezoelectric materials under electromechanical loading is mentioned below. The fracture analysis of an infinitely long piezoelectric ceramic strip, containing a Griffith moving crack with constant velocity was studied by Kwon et al. [5]. Gao et al. [6] addressed an anti-plane problem of moving crack along the interface between two dissimilar piezoelectric medium. The crack is assumed to be permeable crack. Li and Weng [7] analyzed the problem of the moving cracks in a functionally graded piezoelectric material. Meguid et al. [8] considered the problem of a moving crack in an infinite medium with spatially varying elastic properties perpendicular to the direction of the crack propagation. The article by Wang et al. [9] deals with the Yoffe-type moving crack with a constant speed at the interface of two dissimilar piezoelectric half planes by using complex variable technique. The problem of an impermeable moving crack with a constant length propagating in a piezoelectric strip was considered by Li [10]. The cracked piezoelectric layer under the action of uniform anti-plane traction and in-plane electric field. Hu and Zhong [11] considered the fracture behavior of a functionally graded piezoelectric strip containing a constant speed moving crack under impermeable and permeable conditions. Piva et al. [12] solved a transversely isotropic piezoelectric medium with an impermeable and permeable Griffith moving crack under a remote generalized electro-mechanical loading. Yan and Jiang [13] obtained an analytical solution to the moving crack problem in a functionally graded piezoelectric material under an in-plane loading. In another work, the plane problem of two piezoelectric semi-infinite spaces with an interface moving crack under the permeable electric condition with an account of electric traction on its surfaces is investigated by Lapusta et al. [14]. In accord with the above studies, there is not a promising examination regarding the multiple moving cracks interaction with arbitrary arrangement in the piezoelectric materials. The distributed dislocation method has been introduced as a powerful tool to obtain the field intensity factors in the piezoelectric materials weakened by multiple cracks. Li and Lee [15] considered a piezoelectric plane with two collinear unequal cracks under mode-I electromechanical loadings. Asadi [16] employed Volterra climb and glide dislocations to analyze an infinite transversely isotropic piezoelectric plane having co-axial annular cracks under axisymmetric electromechanical loading. The results were used to evaluate field intensity factors for a system of interacting annular and/or penny-shaped cracks. Bagheri et al. [17] provided the calculation of the stress intensity factors for multiple moving cracks in a functionally graded magneto-electro-elastic strip under an anti-plane mechanical and in-plane magneto-electrical loading based on the distribution of screw dislocations. The distributed dislocation technique was also applied to the analysis of a piezoelectric substrate with imperfect functionally graded orthotropic coating (Bagheri et al. [18]) and interface crack in two bonded dissimilar materials (Monfared et al. [19]) in which the interaction of several cracks was studied. Wang and Pan considered the problem of a screw dislocation in functionally graded piezoelectric solids [20]. Monfared and Ayatollahi [21] determined stress and electric displacement intensity factors for several cracks with various configurations in an infinite piezoelectric plane under impermeable and permeable conditions. Bagheri [22] studied the interaction of multiple horizontal cracks in a piezoelectric half-plane under anti-plane transient loading. He employed the distributed dislocation technique to determine the field intensity factors. To our best knowledge, in the previous studies (which deals with the relatively simple problem of cracked functionally graded piezoelectric materials), it is assumed that in the direction(s) parallel to the plane of the crack the material properties does not vary. In the case of fracture of such a nonhomogeneous medium since, generally, the plane of the crack is not a plane of symmetry, and hence the propagating crack would eventually align itself parallel to the direction in which the material properties vary.

In the present study, it is then assumed that the crack is located on the $y = 0$ plane, the material properties are an exponential function of x. However, no solution has been presented for the multiple moving cracks in

functionally graded piezoelectric materials wherein material properties vary exponentially in the plane of the crack direction. The paper is organized as follows: the dislocation solution is accomplished in an FGP plane, wherein the material properties are an exponential function of *x* in section 2. The solution of the mixed-mode problem of multiple moving cracks as well as the solution of the system of integral equations is obtained in section 3. Section 4 contains the numerical results. Finally, concluding remarks are provided in section 5.

2 MOVING ELECTRO-ELASTIC DISLOCATIONS IN AN FGP PLANE

As shown in Fig. 1, the problem under consideration consists of moving electric and Volterra edge dislocations in an FGP plane with properties that vary as a function of coordinate *x*. Although, the jump in the electric potential is not a type of dislocation, it is referred here as the electric potential discontinuity for convenience. It is worth noting that the medium is free of any mechanical and electrical loads. Let *x* and *y*, denote Cartesian coordinates and suppose that a piezoelectric material occupies the entire space except for the region $y=0,\ x>0$, where there are electric and Volterra edge dislocations with the discontinuity strength and Burgers vectors. The electric dislocation is initially assumed to remain open to prevent the transfer of electric potential between its faces. On the other hand, the electro-elastic dislocations obstruct the electric potential as shown in Fig. 1.

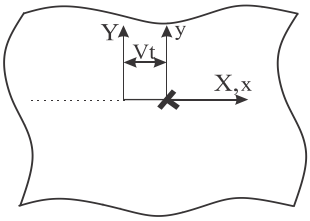

Fig.1
Schematic view of functionally graded piezoelectric plane with moving electro-elastic dislocations.

Field equations for piezoelectric materials are given by [15]

$$\begin{aligned}
\sigma_{XX}(X,Y,t) &= c_{11}(X)\frac{\partial u(X,Y,t)}{\partial X}+c_{13}(X)\frac{\partial v(X,Y,t)}{\partial Y}+e_{31}(X)\frac{\partial \varphi(X,Y,t)}{\partial Y}\\
\sigma_{YY}(X,Y,t) &= c_{13}(X)\frac{\partial u(X,Y,t)}{\partial X}+c_{33}(X)\frac{\partial v(X,Y,t)}{\partial Y}+e_{33}(X)\frac{\partial \varphi(X,Y,t)}{\partial Y}\\
\sigma_{XY}(X,Y,t) &= c_{44}(X)\left(\frac{\partial u(X,Y,t)}{\partial Y}+\frac{\partial v(X,Y,t)}{\partial X}\right)+e_{15}(X)\frac{\partial \varphi(X,Y,t)}{\partial X}\\
D_X(X,Y,t) &= e_{15}(X)\left(\frac{\partial u(X,Y,t)}{\partial Y}+\frac{\partial v(X,Y,t)}{\partial X}\right)-\varepsilon_{11}(X)\frac{\partial \varphi(X,Y,t)}{\partial X}\\
D_Y(X,Y,t) &= e_{31}(X)\frac{\partial u(X,Y,t)}{\partial X}+e_{33}(X)\frac{\partial v(X,Y,t)}{\partial Y}-\varepsilon_{33}(X)\frac{\partial \varphi(X,Y,t)}{\partial Y}
\end{aligned} \tag{1}$$

where σ_{XX}, σ_{YY} and σ_{XY} are the in-plane stress tensors, D_X and D_Y are the in-plane electric displacements. Also, $c_{11}(X), c_{13}(X), c_{33}(X)$ and $c_{44}(X)$ are the elastic modules, $e_{31}(X)$, $e_{33}(X)$ and $e_{15}(X)$ are the piezoelectric parameters, and $\varepsilon_{11}(X)$ and $\varepsilon_{33}(X)$ are the dielectric permittivity of the FGPMs. Crack problems in the non-homogeneous piezoelectric materials do not appear to be analytically tractable for arbitrary variations of material properties. To this end, it is a general practice to adopt suitable mathematical functions to represent the variation in properties for which the problem becomes tractable. Similar to the treatment of the crack problem for isotropic non-homogeneous materials [23], we assume that the material gradient is oriented along the *x*-direction and the electro-elastic properties depend on the horizontal coordinate *X* as follows:

$$\begin{aligned}
&c_{11}(X)=c_{110}e^{\beta X}, c_{13}(X)=c_{130}e^{\beta X}, c_{33}(X)=c_{330}e^{\beta X}, c_{44}(X)=c_{440}e^{\beta X}, e_{31}(X)=e_{310}e^{\beta X},\\
&e_{33}(X)=e_{330}e^{\beta X}, e_{15}(X)=e_{150}e^{\beta X}, \varepsilon_{11}(X)=\varepsilon_{110}e^{\beta X}, \varepsilon_{33}(X)=\varepsilon_{330}e^{\beta X}
\end{aligned} \tag{2}$$

where c_{ij0} are the elastic modules, e_{ij0} are the piezoelectric parameters, and ε_{ij0} are the dielectric permittivity at $X=0$ and β is a positive or negative constant. By neglecting body forces and electric charge density, the equations of motion and Maxwell equation for the FGPMs are expressed by

$$\begin{aligned}
&c_{110}\frac{\partial^2 u}{\partial X^2}+(c_{130}+c_{440})\frac{\partial^2 v}{\partial X\,\partial Y}+c_{440}\frac{\partial^2 u}{\partial Y^2}+(e_{310}+e_{150})\frac{\partial^2 \varphi}{\partial X\,\partial Y}+\beta(c_{110}\frac{\partial u}{\partial X}+c_{130}\frac{\partial v}{\partial Y}+e_{310}\frac{\partial \varphi}{\partial Y})=\rho_0\frac{\partial^2 u}{\partial t^2},\\
&c_{440}\frac{\partial^2 v}{\partial X^2}+(c_{130}+c_{440})\frac{\partial^2 u}{\partial X\,\partial Y}+c_{330}\frac{\partial^2 v}{\partial Y^2}+e_{150}\frac{\partial^2 \varphi}{\partial X^2}+e_{330}\frac{\partial^2 \varphi}{\partial Y^2}+\beta c_{440}(\frac{\partial u}{\partial Y}+\frac{\partial v}{\partial X})+\beta e_{150}\frac{\partial \varphi}{\partial X}=\rho_0\frac{\partial^2 v}{\partial t^2},\\
&-\varepsilon_{110}\frac{\partial^2 \varphi}{\partial X^2}-\varepsilon_{330}\frac{\partial^2 \varphi}{\partial Y^2}+e_{150}\frac{\partial^2 v}{\partial X^2}+e_{330}\frac{\partial^2 v}{\partial Y^2}+(e_{310}+e_{150})\frac{\partial^2 u}{\partial X\,\partial Y}+\beta e_{150}(\frac{\partial u}{\partial Y}+\frac{\partial v}{\partial X})-\beta\varepsilon_{110}\frac{\partial \varphi}{\partial X}=0.
\end{aligned}\tag{3}$$

Let us now assume that the variation of mass density in the medium are defined by $\rho(X)=\rho_0 e^{\beta X}$, where ρ_0 is the density $X=0$. It is usually convenient to study the crack propagation in a moving coordinate system (x,y,t), with [12]

$$x=X-Vt,\ y=Y,\ z=Z,\tag{4}$$

where (x,y,t) represents the moving coordinate system, attached to the moving dislocation. By making use of (4), the equations of motion in the moving coordinate system are cast into the form:

$$\begin{aligned}
&(c_{110}-\rho_0 V^2)\frac{\partial^2 u}{\partial x^2}+(c_{130}+c_{440})\frac{\partial^2 v}{\partial x\,\partial y}+c_{440}\frac{\partial^2 u}{\partial y^2}+(e_{310}+e_{150})\frac{\partial^2 \varphi}{\partial x\,\partial y}+\beta(c_{110}\frac{\partial u}{\partial x}+c_{130}\frac{\partial v}{\partial y}+e_{310}\frac{\partial \varphi}{\partial y})=0,\\
&(c_{440}-\rho_0 V^2)\frac{\partial^2 v}{\partial x^2}+(c_{130}+c_{440})\frac{\partial^2 u}{\partial x\,\partial y}+c_{330}\frac{\partial^2 v}{\partial y^2}+e_{150}\frac{\partial^2 \varphi}{\partial x^2}+e_{330}\frac{\partial^2 \varphi}{\partial y^2}+\beta c_{440}(\frac{\partial u}{\partial y}+\frac{\partial v}{\partial x})+\beta e_{150}\frac{\partial \varphi}{\partial x}=0,\\
&-\varepsilon_{110}\frac{\partial^2 \varphi}{\partial x^2}-\varepsilon_{330}\frac{\partial^2 \varphi}{\partial y^2}+e_{150}\frac{\partial^2 v}{\partial x^2}+e_{330}\frac{\partial^2 v}{\partial y^2}+(e_{310}+e_{150})\frac{\partial^2 u}{\partial x\,\partial y}+\beta e_{150}(\frac{\partial u}{\partial y}+\frac{\partial v}{\partial x})-\beta\varepsilon_{110}\frac{\partial \varphi}{\partial x}=0.
\end{aligned}\tag{5}$$

The issue of how to impose the electrical boundary conditions along the crack surfaces in piezoelectric fracture modeling is a controversial one. Here we consider impermeable boundary conditions. To obtain the solution of moving electric and Volterra edge dislocations, we locate an edge dislocation at the origin and let the line of electrical potential discontinuity be the dislocation cut; thus, the electromechanical boundary conditions at the dislocations path can be stated in the form:

$$\begin{aligned}
&u(x,0^+)-u(x,0^-)=b_x H(x),\quad v(x,0^+)-v(x,0^-)=b_y H(x),\quad \varphi(x,0^+)-\varphi(x,0^-)=b_\varphi H(x),\\
&\sigma_{yy}(x,0^+)=\sigma_{yy}(x,0^-),\quad \sigma_{xy}(x,0^+)=\sigma_{xy}(x,0^-),\quad D_y(x,0^+)=D_y(x,0^-).
\end{aligned}\tag{6}$$

where $H(.)$ is the Heaviside step function and b_x, b_y and b_φ are the displacement, electric potential and magnetic potential jumps across the dislocation cut, respectively. By using the standard Fourier transform, the solution of the problem (5) may be obtained as:

$$\begin{aligned}
&\frac{d^2U^*}{dy^2}+(\beta\alpha_1+i\zeta\alpha_2)\frac{dV^*}{dy}+(i\zeta(\alpha_5+\alpha_7)+\beta\alpha_5)\frac{d\Phi^*}{dy}+((k^2-\alpha_3)\zeta^2+i\beta\zeta\alpha_3)U^*=0\\
&\alpha_4\frac{d^2V^*}{dy^2}+(i\zeta\alpha_2+\beta)\frac{dU^*}{dy}+\alpha_6\frac{d^2\Phi^*}{dy^2}+(i\zeta\beta\alpha_7-\alpha_7\zeta^2)\Phi^*+((k^2-1)\zeta^2+i\beta\zeta)V^*=0\\
&-\alpha_8\frac{d^2\Phi^*}{dy^2}+\alpha_6\frac{d^2V^*}{dy^2}+(i\zeta(\alpha_5+\alpha_7)+\beta\alpha_7)\frac{dU^*}{dy}+(\alpha_9\zeta^2-i\beta\zeta\alpha_9)\Phi^*+(i\beta\zeta\alpha_7-\alpha_7\zeta^2)V^*=0
\end{aligned}\tag{7}$$

where $i=\sqrt{-1}$, ζ is Fourier variable, U, V and Φ are Fourier transforms of displacement components u, v and electrical potential φ respectively, and k, $\alpha_i,(i=1,2,...,9)$ are represented in the Appendix I. The solution of the problem satisfying the necessary far field conditions of displacement components and electrical potential may be expressed as:

$$U^*(\zeta,y)=\sum_{j=1}^{3}A_j(\zeta)e^{\lambda_j y},\quad V^*(\zeta,y)=\sum_{j=1}^{3}m_jA_j(\zeta)e^{\lambda_j y},\quad \Phi^*(\zeta,y)=\sum_{j=1}^{3}n_jA_j(\zeta)e^{\lambda_j y} \tag{8}$$

where

$$m_j=\frac{r_1\lambda_j^4+r_2\lambda_j^2+r_3}{r_4\lambda_j^3+r_5\lambda_j},\quad n_j=-\frac{\lambda_j{}^2+m_j(\beta\alpha_1+i\zeta\alpha_2)\lambda_j+(k^2-\alpha_3)\zeta^2+i\beta\zeta\alpha_3}{[\beta\alpha_5+i\zeta(\alpha_5+\alpha_7)]\lambda_j},\quad j\in\{1,2,3\} \tag{9}$$

Moreover, $r_i,(i=1,2,...,5)$ are appeared in Appendix II. In Eqs. (9), functions $A_j,(j=1,2,3)$ are arbitrary unknowns. The characteristic equation and its roots are found to be:

$$\lambda^6-\Delta_1\lambda^4+\Delta_2\lambda^2-\Delta_3=0, \tag{10}$$

The solution to (10) is found to be

$$\begin{aligned}&\lambda_1=-\sqrt{\frac{\Delta_1}{3}+\frac{2^{1/3}p}{3(q+r)^{1/3}}+\frac{(q+r)^{1/3}}{3\times2^{1/3}}},\quad \lambda_2=-\sqrt{\frac{\Delta_1}{3}-\frac{(1+i\sqrt{3})p}{3\times2^{2/3}(q+r)^{1/3}}+\frac{(-1+i\sqrt{3})(q+r)^{1/3}}{6\times2^{1/3}}},\\&\lambda_3=-\sqrt{\frac{\Delta_1}{3}-\frac{(1-i\sqrt{3})p}{3\times2^{2/3}(q+r)^{1/3}}-\frac{(1+i\sqrt{3})(q+r)^{1/3}}{6\times2^{1/3}}}\end{aligned} \tag{11}$$

where

$$\begin{aligned}&p=\Delta_1{}^2-3\Delta_2,\ q=2\Delta_1{}^3-9\Delta_1\Delta_2+27\Delta_3,\ r=\sqrt{-4p^3+q^2},\\&\Delta_1=\frac{\alpha_4H_8+\alpha_6(-2H_6+H_2H_7-H_1\alpha_6)+H_3(-H_7\alpha_4+H_4\alpha_6)+\alpha_8(H_2H_4-H_5-H_1\alpha_4)}{\alpha_4\alpha_8+\alpha_6{}^2},\\&\Delta_2=\frac{H_6{}^2+H_3(H_5H_7-H_4H_6)+H_2H_4H_8-H_5H_8-H_1H_8\alpha_4+H_6(2H_1\alpha_6-H_2H_7)+H_1H_5\alpha_8}{\alpha_4\alpha_8+\alpha_6{}^2},\\&\Delta_3=\frac{H_1(-H_6{}^2+H_5H_8)}{\alpha_4\alpha_8+\alpha_6{}^2},\end{aligned} \tag{12}$$

In addition, the functions $H_i,(i=1,2,...,8)$ are given in Appendix II. By using the inverse Fourier transform, the displacement fields and electrical potential (8) may be written as:

$$\begin{aligned}&u(x,y)=\frac{1}{2\pi}\int_{-\infty}^{\infty}(\sum_{j=1}^{3}A_je^{\lambda_j y})e^{i\zeta x}d\zeta,\quad v(x,y)=\frac{1}{2\pi}\int_{-\infty}^{\infty}(\sum_{j=1}^{3}m_jA_je^{\lambda_j y})e^{i\zeta x}d\zeta,\\&\varphi(x,y)=\frac{1}{2\pi}\int_{-\infty}^{\infty}(\sum_{j=1}^{3}n_jA_je^{\lambda_j y})e^{i\zeta x}d\zeta\end{aligned} \tag{13}$$

From (1), (2), (4) and (13) it then follows that

$$\sigma_{xx}(x,y)=\frac{e^{\beta X}c_{440}}{2\pi}\int_{-\infty}^{\infty}(\sum_{j=1}^{3}b_{1j}A_j e^{\lambda_j y})e^{i\zeta x}d\zeta,\ \ \sigma_{yy}(x,y)=\frac{e^{\beta X}c_{440}}{2\pi}\int_{-\infty}^{\infty}(\sum_{j=1}^{3}b_{2j}A_j e^{\lambda_j y})e^{i\zeta x}d\zeta$$
$$\sigma_{xy}(x,y)=\frac{e^{\beta X}c_{440}}{2\pi}\int_{-\infty}^{\infty}(\sum_{j=1}^{3}b_{3j}A_j e^{\lambda_j y})e^{i\zeta x}d\zeta,\ \ D_x(x,y)=\frac{e^{\beta X}c_{440}}{2\pi}\int_{-\infty}^{\infty}(\sum_{j=1}^{3}b_{4j}A_j e^{\lambda_j y})e^{i\zeta x}d\zeta \quad (14)$$
$$D_y(x,y)=\frac{e^{\beta X}c_{440}}{2\pi}\int_{-\infty}^{\infty}(\sum_{j=1}^{3}b_{5j}A_j e^{\lambda_j y})e^{i\zeta x}d\zeta$$

where

$$b_{1j}=\zeta\alpha_3+\alpha_1 m_j\lambda_j+\alpha_5 n_j\lambda_j,\ b_{2j}=\zeta\alpha_1+\alpha_4 m_j\lambda_j+\alpha_6 n_j\lambda_j,\ b_{3j}=\lambda_j-\zeta m_j-\zeta\alpha_7 n_j$$
$$b_{4j}=\alpha_7\lambda_j-\zeta\alpha_7 m_j+\zeta\alpha_9 n_j,\ b_{5j}=\zeta\alpha_5+\alpha_6 m_j\lambda_j-\alpha_8 n_j\lambda_j \qquad j=1,2,3 \quad (15)$$

From (7), (8), (13) and (14), the unknown functions $A_i(\zeta), i=\{1,2,3\}$ may be obtained as follows:

$$A_1(\zeta)=\frac{(\pi\delta(\zeta)-i/\zeta)}{2}(A_{11}b_x+A_{12}b_y+A_{13}b_\varphi),\quad A_2(\zeta)=\frac{(\pi\delta(\zeta)-i/\zeta)}{2}(A_{21}b_x+A_{22}b_y+A_{23}b_\varphi)$$
$$A_3(\zeta)=\frac{(\pi\delta(\zeta)-i/\zeta)}{2}(A_{31}b_x+A_{32}b_y+A_{33}b_\varphi) \quad (16)$$

where $\delta(.)$ is the Dirac delta function and the functions $A_{ij}, i,j\in\{1,2,3\}$ are given in Appendix II. Substituting unknown functions (16) into the stress fields and electric displacements (14), it may easily be shown that

$$\sigma_{xx}(x,y)=\frac{e^{\beta X}c_{440}}{4}[b_x\sum_{j=1}^{3}b_{1j}A_{j1}e^{\lambda_j y}+b_y\sum_{j=1}^{3}b_{1j}A_{j2}e^{\lambda_j y}+b_\varphi\sum_{j=1}^{3}b_{1j}A_{j3}e^{\lambda_j y}]\Big|_{\zeta=0}+\int_{-\infty}^{\infty}f_{xx}(x,y,\zeta)d\zeta$$
$$\sigma_{yy}(x,y)=\frac{e^{\beta X}c_{440}}{4}[b_x\sum_{j=1}^{3}b_{2j}A_{j1}e^{\lambda_j y}+b_y\sum_{j=1}^{3}b_{2j}A_{j2}e^{\lambda_j y}+b_\varphi\sum_{j=1}^{3}b_{2j}A_{j3}e^{\lambda_j y}]\Big|_{\zeta=0}+\int_{-\infty}^{\infty}f_{yy}(x,y,\zeta)d\zeta$$
$$\sigma_{xy}(x,y)=\frac{e^{\beta X}c_{440}}{4}[b_x\sum_{j=1}^{3}b_{3j}A_{j1}e^{\lambda_j y}+b_y\sum_{j=1}^{3}b_{3j}A_{j2}e^{\lambda_j y}+b_\varphi\sum_{j=1}^{3}b_{3j}A_{j3}e^{\lambda_j y}]\Big|_{\zeta=0}+\int_{-\infty}^{\infty}f_{xy}(x,y,\zeta)d\zeta \quad (17)$$
$$D_x(x,y)=\frac{e^{\beta X}c_{440}}{4}[b_x\sum_{j=1}^{3}b_{4j}A_{j1}e^{\lambda_j y}+b_y\sum_{j=1}^{3}b_{4j}A_{j2}e^{\lambda_j y}+b_\varphi\sum_{j=1}^{3}b_{4j}A_{j3}e^{\lambda_j y}]\Big|_{\zeta=0}+\int_{-\infty}^{\infty}f_{dx}(x,y,\zeta)d\zeta$$
$$D_y(x,y)=\frac{e^{\beta X}c_{440}}{4}[b_x\sum_{j=1}^{3}b_{5j}A_{j1}e^{\lambda_j y}+b_y\sum_{j=1}^{3}b_{5j}A_{j2}e^{\lambda_j y}+b_\varphi\sum_{j=1}^{3}b_{5j}A_{j3}e^{\lambda_j y}]\Big|_{\zeta=0}+\int_{-\infty}^{\infty}f_{dy}(x,y,\zeta)d\zeta$$

where $f_{ij}(x,y,\zeta), i\in\{x,y,d\}, j\in\{x,y\}$ are defined in Appendix II. The singular behavior of the kernels f_{ij} may be obtained from the asymptotic analysis of the integrals in (17). In this case through an asymptotic analysis the singular part of the kernel can be separated and it can be shown that the integral equation has the standard Cauchy kernel. By adding and subtracting the asymptotic expressions of the integrands using asymptotic expressions for large value ζ, we find:

$$f_{ij}(x,y,\zeta)=\underbrace{f_{ij\infty}(x,y,\zeta)}_{Singular\ Part}+\underbrace{[f_{ij}(x,y,\zeta)-f_{ij\infty}(x,y,\zeta)]}_{Non\ singular\ Part} \quad (18)$$

The stress fields and electric displacement components (17) by view of Eq. (18) and after very lengthy analysis, lead to

$$\sigma_{xx}(x,y)=\frac{e^{\beta X}c_{440}}{4}[b_x\sum_{j=1}^{3}b_{1j}A_{j1}e^{\lambda_j y}+b_y\sum_{j=1}^{3}b_{1j}A_{j2}e^{\lambda_j y}+b_\varphi\sum_{j=1}^{3}b_{1j}A_{j3}e^{\lambda_j y}]\Big|_{\zeta=0}+\frac{e^{\beta X}c_{440}}{2\pi}\{b_x[\frac{\gamma_1\eta_1\lambda_{11}y}{x^2+(\lambda_{11}y)^2}+\frac{\gamma_2\eta_2\lambda_{22}y}{x^2+(\lambda_{22}y)^2}+\frac{\gamma_3\eta_3\lambda_{33}y}{x^2+(\lambda_{33}y)^2}]-b_y[\frac{\gamma_4\eta_1 x}{x^2+(\lambda_{11}y)^2}+\frac{\gamma_5\eta_2 x}{x^2+(\lambda_{22}y)^2}+\frac{\gamma_6\eta_3 x}{x^2+(\lambda_{33}y)^2}]-b_\varphi[\frac{\gamma_7\eta_1 x}{x^2+(\lambda_{11}y)^2}+\frac{\gamma_8\eta_2 x}{x^2+(\lambda_{22}y)^2}+\frac{\gamma_9\eta_3 x}{x^2+(\lambda_{33}y)^2}]\}+\int_{-\infty}^{\infty}[f_{xx}(x,y,\zeta)-f_{xx\infty}(x,y,\zeta)]d\zeta$$

$$\sigma_{yy}(x,y)=\frac{e^{\beta X}c_{440}}{4}[b_x\sum_{j=1}^{3}b_{2j}A_{j1}e^{\lambda_j y}+b_y\sum_{j=1}^{3}b_{2j}A_{j2}e^{\lambda_j y}+b_\varphi\sum_{j=1}^{3}b_{2j}A_{j3}e^{\lambda_j y}]\Big|_{\zeta=0}+\frac{e^{\beta X}c_{440}}{2\pi}\{b_x[\frac{\gamma_1\eta_4\lambda_{11}y}{x^2+(\lambda_{11}y)^2}+\frac{\gamma_2\eta_5\lambda_{22}y}{x^2+(\lambda_{22}y)^2}+\frac{\gamma_3\eta_6\lambda_{33}y}{x^2+(\lambda_{33}y)^2}]-b_y[\frac{\gamma_4\eta_4 x}{x^2+(\lambda_{11}y)^2}+\frac{\gamma_5\eta_5 x}{x^2+(\lambda_{22}y)^2}+\frac{\gamma_6\eta_6 x}{x^2+(\lambda_{33}y)^2}]-b_\varphi[\frac{\gamma_7\eta_4 x}{x^2+(\lambda_{11}y)^2}+\frac{\gamma_8\eta_5 x}{x^2+(\lambda_{22}y)^2}+\frac{\gamma_9\eta_6 x}{x^2+(\lambda_{33}y)^2}]\}+\int_{-\infty}^{\infty}[f_{yy}(x,y,\zeta)-f_{yy\infty}(x,y,\zeta)]d\zeta$$

$$\sigma_{xy}(x,y)=\frac{e^{\beta X}c_{440}}{4}[b_x\sum_{j=1}^{3}b_{3j}A_{j1}e^{\lambda_j y}+b_y\sum_{j=1}^{3}b_{3j}A_{j2}e^{\lambda_j y}+b_\varphi\sum_{j=1}^{3}b_{3j}A_{j3}e^{\lambda_j y}]\Big|_{\zeta=0}-\frac{e^{\beta X}c_{440}}{2\pi}\{b_x[\frac{\gamma_1\eta_7 x}{x^2+(\lambda_{11}y)^2}+\frac{\gamma_2\eta_8 x}{x^2+(\lambda_{22}y)^2}+\frac{\gamma_3\eta_9 x}{x^2+(\lambda_{33}y)^2}]+b_y[\frac{\gamma_4\eta_7\lambda_{11}y}{x^2+(\lambda_{11}y)^2}+\frac{\gamma_5\eta_8\lambda_{22}y}{x^2+(\lambda_{22}y)^2}+\frac{\gamma_6\eta_9\lambda_{33}y}{x^2+(\lambda_{33}y)^2}]+b_\varphi[\frac{\gamma_7\eta_7\lambda_{11}y}{x^2+(\lambda_{11}y)^2}+\frac{\gamma_8\eta_8\lambda_{22}y}{x^2+(\lambda_{22}y)^2}+\frac{\gamma_9\eta_9\lambda_{33}y}{x^2+(\lambda_{33}y)^2}]\}+\int_{-\infty}^{\infty}[f_{xy}(x,y,\zeta)-f_{xy\infty}(x,y,\zeta)]d\zeta \tag{19}$$

$$D_x(x,y)=\frac{e^{\beta X}c_{440}}{4}[b_x\sum_{j=1}^{3}b_{4j}A_{j1}e^{\lambda_j y}+b_y\sum_{j=1}^{3}b_{4j}A_{j2}e^{\lambda_j y}+b_\varphi\sum_{j=1}^{3}b_{4j}A_{j3}e^{\lambda_j y}]\Big|_{\zeta=0}-\frac{e^{\beta X}c_{440}}{2\pi}\{b_x[\frac{\gamma_1\eta_{10}x}{x^2+(\lambda_{11}y)^2}+\frac{\gamma_2\eta_{11}x}{x^2+(\lambda_{22}y)^2}+\frac{\gamma_3\eta_{12}x}{x^2+(\lambda_{33}y)^2}]+b_y[\frac{\gamma_4\eta_{10}\lambda_{11}y}{x^2+(\lambda_{11}y)^2}+\frac{\gamma_5\eta_{11}\lambda_{22}y}{x^2+(\lambda_{22}y)^2}+\frac{\gamma_6\eta_{12}\lambda_{33}y}{x^2+(\lambda_{33}y)^2}]+b_\varphi[\frac{\gamma_7\eta_{10}\lambda_{11}y}{x^2+(\lambda_{11}y)^2}+\frac{\gamma_8\eta_{11}\lambda_{22}y}{x^2+(\lambda_{22}y)^2}+\frac{\gamma_9\eta_{12}\lambda_{33}y}{x^2+(\lambda_{33}y)^2}]\}+\int_{-\infty}^{\infty}[f_{dx}(x,y,\zeta)-f_{dx\infty}(x,y,\zeta)]d\zeta$$

$$D_y(x,y)=\frac{e^{\beta X}c_{440}}{4}[b_x\sum_{j=1}^{3}b_{5j}A_{j1}e^{\lambda_j y}+b_y\sum_{j=1}^{3}b_{5j}A_{j2}e^{\lambda_j y}+b_\varphi\sum_{j=1}^{3}b_{5j}A_{j3}e^{\lambda_j y}]\Big|_{\zeta=0}+\frac{e^{\beta X}c_{440}}{2\pi}\{b_x[\frac{\gamma_1\eta_{13}\lambda_{11}y}{x^2+(\lambda_{11}y)^2}+\frac{\gamma_2\eta_{14}\lambda_{22}y}{x^2+(\lambda_{22}y)^2}+\frac{\gamma_3\eta_{15}\lambda_{33}y}{x^2+(\lambda_{33}y)^2}]-b_y[\frac{\gamma_4\eta_{13}x}{x^2+(\lambda_{11}y)^2}+\frac{\gamma_5\eta_{14}x}{x^2+(\lambda_{22}y)^2}+\frac{\gamma_6\eta_{15}x}{x^2+(\lambda_{33}y)^2}]-b_\varphi[\frac{\gamma_7\eta_{13}x}{x^2+(\lambda_{11}y)^2}+\frac{\gamma_8\eta_{14}x}{x^2+(\lambda_{22}y)^2}+\frac{\gamma_9\eta_{15}x}{x^2+(\lambda_{33}y)^2}]\}+\int_{-\infty}^{\infty}[f_{dy}(x,y,s,\zeta)-f_{dy\infty}(x,y,s,\zeta)]d\zeta$$

where $f_{ij\infty}(x,y,\zeta), i\in\{x,y,d\}, j\in\{x,y\}$, $\gamma_i, i\in\{1,2,...,9\}$ and $\eta_i, i\in\{1,2,...,15\}$ are given in Appendix III. It can be seen from Eqs (19) that the stress and electric displacement components exhibit the familiar Cauchy-type singularity at the locations of electro-elastic dislocation. It is worth mentioning that Eq. (19) may be used as Green's function to determine stress and electric displacement fields in a FGP medium subjected to any distribution of self-equilibrating traction.

3 ANALYSIS OF MULTIPLE MOVING CRACKS

In this section, we will introduce, and apply, the distributed dislocation technique for modeling the moving cracks in FGPM. The present problem can be treated as the superposition of two-sub problem. First, the stress state and electric displacement induced in the uncracked medium is found. Then, the stress and electric displacement due to a continuous distribution of electro-elastic dislocations along the crack-line are obtained without external loadings; this is the "correct solution". The crack faces subjected to the distributed dislocations cancel out the stress and electric displacement induced by the first problem. In the framework of linear theory, the sum of the two solutions corresponding is the solution to the original problem. The geometry of crack is presented in parametric form as:

$$x_i(p)=x_{ic}+pl_i, \qquad y_i(p)=y_{ic}, \qquad -1\le p\le 1, \quad i\in\{1,2,3,...,N\} \tag{20}$$

where (x_{ic}, y_{ic}) and l_i are the coordinates of the center and a half length of the *i-th* cracks, respectively. The total traction and electric displacement on the crack face due to the electro-elastic solution and the dislocation distributions can then be written as:

$$\begin{aligned}
\sigma_{yy}(x_i(p),y_i(p)) &= \sum_{k=1}^{N}\int_{-1}^{1}[k_{ik}^{11}(p,q)b_{xk}(q)+k_{ik}^{12}(p,q)b_{yk}(q)+k_{ik}^{13}(p,q)b_{\varphi k}(q)]dq\\
\sigma_{xy}(x_i(p),y_i(p)) &= \sum_{k=1}^{N}\int_{-1}^{1}[k_{ik}^{21}(p,q)b_{xk}(q)+k_{ik}^{22}(p,q)b_{yk}(q)+k_{ik}^{23}(p,q)b_{\varphi k}(q)]dq\\
D_y(x_i(p),y_i(p)) &= \sum_{k=1}^{N}\int_{-1}^{1}[k_{ik}^{31}(p,q)b_{xk}(q)+k_{ik}^{32}(p,q)b_{yk}(q)+k_{ik}^{33}(p,q)b_{\varphi k}(q)]dq
\end{aligned} \tag{21}$$

where $b_{xk}(q)$, $b_{yk}(q)$ and $b_{\varphi k}(q)$ are the dislocation density functions on the face of *k-th* crack, $k_{ik}^{lm}, l,m=1,2,3, i,k=x,y,d$ are coefficients of b_x, b_y and b_φ in Eq. (19). The kernels in Eq. (21) exhibit Cauchy type singularity for $i=k$ as $q\to p$ and may be expressed as:

$$k_{ii}^{kl}(p,q)=\frac{a_{kl,-1i}(q)}{p-q}+\sum_{m=0}^{\infty}a_{kl,mi}(q)(p-q)^m, \quad k,l=1,2,3, k=x,y,d \tag{22}$$

The coefficients of singular terms $a_{kl,-1i}(q)$ can be obtained by means of the Taylor series expansion of $x_i(q)$ and $y_i(q)$ in the vicinity of *q* and are

$$\begin{aligned}
&a_{11,-1i}=0,\ a_{12,-1i}=-\frac{c_{440}}{2\pi l_i}\sum_{j=1}^{3}\gamma_{j+3}\eta_{j+3},\ a_{13,-1i}=-\frac{c_{440}}{2\pi l_i}\sum_{j=1}^{3}\gamma_{j+6}\eta_{j+3}\\
&a_{21,-1i}=-\frac{c_{440}}{2\pi l_i}\sum_{j=1}^{3}\gamma_j\eta_{j+6},\ a_{22,-1i}=0,\ a_{23,-1i}=0\\
&a_{31,-1i}=0,\ a_{32,-1i}=-\frac{c_{440}}{2\pi l_i}\sum_{j=1}^{3}\gamma_{j+3}\eta_{j+12},\ a_{33,-1i}=-\frac{c_{440}}{2\pi l_i}\sum_{j=1}^{3}\gamma_{j+6}\eta_{j+12},
\end{aligned} \tag{23}$$

It is also necessary to impose the closure conditions to enforce single-valued conditions out of each crack faces:

$$\int_{-1}^{1}b_{kj}(q)dq=0,\ k\in\{x,y,d\},\ j\in\{1,2,...,N\} \tag{24}$$

By observing that the fundamental solution of the stress fields and the electric displacements has a square root singularity at crack tips, the unknown dislocation densities on the surface of impermeable cracks, are taken as (Delale and Erdogan [23])

$$b_{ki}(q)=\frac{g_{ki}(q)e^{-\beta X}}{\sqrt{1-q^2}},\ k\in\{x,y,d\},\ -1<q<1,\ i\in\{1,2,...,N\} \tag{25}$$

By replacing Eqs. (25) into Eqs. (21) and (24), and using the Lobatto–Chebyshev integration formula, the discretization singular integral equations lead to

$$\int_{-1}^{1} k_{myij}^{1h}(p,q)\frac{g_{ij}(q)}{\sqrt{1-q^2}}dq=\frac{\pi}{n-1}\sum_{r=1}^{n}e_r k_{myij}^{1h}(p_l,q_r)g_{ij}(q_r),\quad m\in\{x,y,d\},\ h\in\{1,2,3\} \tag{26}$$

where the collocation points are chosen as $q_r=\cos[\frac{(r-1)\pi}{n-1}],\ r\in\{1,2,...,n\}$, $p_l=\cos[\frac{(2l-1)\pi}{2(n-1)}],\ l\in\{1,2,...,n-1\}$, $e_r=0.5$ for $r=1,n$ and $e_r=1$ for $1<r<n$. The field intensity factors for a crack are obtained by Bagheri and Noroozi [24].

4 RESULTS AND DISCUSSION

In this section, in order to investigate the effects of the crack moving velocity, the functionally graded material parameter and the applied electric and magnetic loading on the field intensity factors, we carried out some numerical works. In the computational procedure, the material properties used in the numerical examples are given in Table 1. To study the effect of electro-elastic interaction, the electric loading parameter is introduced as $\lambda_D=e_{150}D_0/\sigma_0\varepsilon_{110}$. The modes I and II stress-intensity factors are normalized by $k_0=\sigma_0\sqrt{l}$ and $k_0=\tau_0\sqrt{l}$ respectively, for a crack in an infinite plane, where l is the half length of the crack. Also, the electric displacement is normalized by $k_{0D}=e_{330}\sqrt{l}/c_{330}$.

Table 1
The relevant material properties PZT-6B.

$c_{110}\times10^{10}$ $(\frac{N}{m^2})$	$c_{130}\times10^{10}$ $(\frac{N}{m^2})$	$c_{330}\times10^{10}$ $(\frac{N}{m^2})$	$c_{440}\times10^{10}$ $(\frac{N}{m^2})$	e_{310} $(\frac{C}{m^2})$	e_{330} $(\frac{C}{m^2})$	e_{150} $(\frac{C}{m^2})$	$\varepsilon_{110}\times10^{-10}$ $(\frac{C}{Vm})$	$\varepsilon_{330}\times10^{-10}$ $(\frac{C}{Vm})$	ρ $(\frac{kg}{m^3})$
16.8	6	16.3	2.71	-0.9	7.1	4.6	36	34	7550

The first example deals with the verification of the resulting analytical solutions. To verify the validity of formulation, the problem of an FG elastic plane under constant far-field applied traction weakened by a straight crack is examined. The stationary crack is subjected to the in-plane constant normal traction. The SIFs are in excellent agreement with those obtained by Delale and Erdogan (Fig. 2(b)).

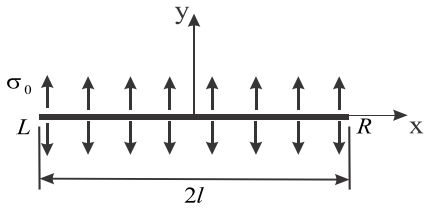

(a)

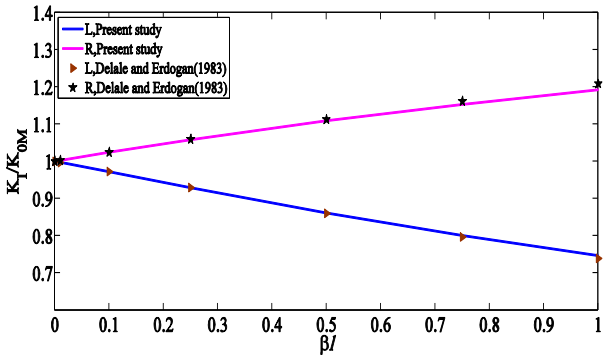

(b)

Fig.2
Comparison of Mode I stress intensity factors of the non-homogeneous elastic material with [23].

The preceding formulation lets the analysis of any number of parallel cracks subjected to mixed mode mechanical and electrical loads.

4.1 Single moving crack

The variation of normalized SIFs in an FGP plane containing a moving crack and subject to three different gradient material properties is shown in Fig. 3(b). The magnitude of the electric loading parameter is chosen as $\lambda_D = 0.1$. It is observed that, the normalized SIFs of the right tip of the crack increases as the crack moving velocity increases, and for the same crack moving velocity the increase of the functionally graded parameter leads to larger SIF values. For the left tip of the crack, the foregoing argument does not hold. Finally, the results of the SIFs for the right crack tip, which is situated in a stiffer zone, is higher than the SIF of the left crack tip. This, of course, is the well-known result in fracture mechanics. The phenomenon was reported by other researchers see e.g. (Delale and Erdogan). It can be seen from Fig. 3(c) that the normalized electric displacement intensity factors vary as the crack speed changes. The EDIFs increases with increasing of the crack propagation speed. In this case, the effect of the gradient property upon EDIFs of the crack tips is not considerably with respect to the SIFs. The influence of the crack speed becomes larger when the ratio of V/c increases. However, the influence of crack speed is dominant only when V/c is in the range between 0.6 and 0.9. When the value of V/c being smaller than 0.6 its influence becomes very weak.

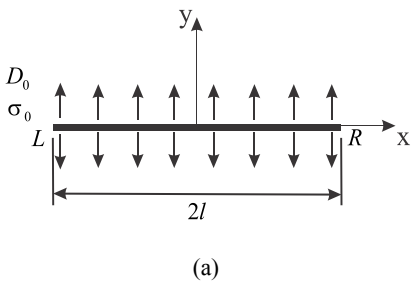

(a)

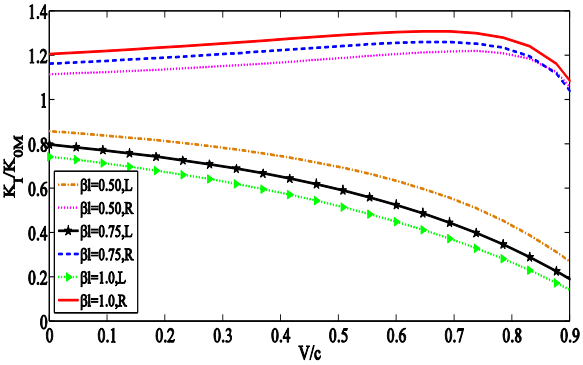

(b)

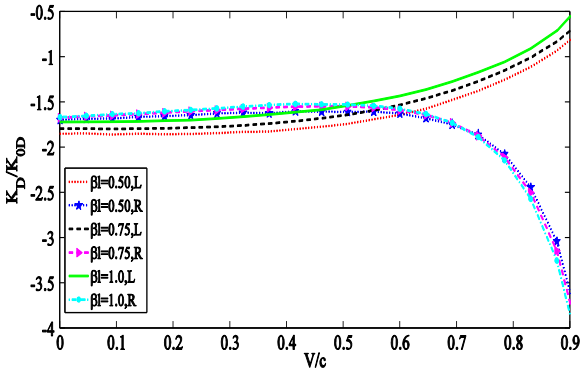

(c)

Fig.3
(b) Variations of Mode I SIFs of a crack versus the graded parameter. (c) Variations of EDIFs of a crack with the graded parameter.

It is interesting to investigate the influence of mechanical and electric loading parameter on the normalized field intensity factors. Figs. 4(b), 4(c), and 4(d) show the variations of mode I, mode II SIFs (K_I, K_{II}) and EDIF (K_D) with electromechanical coupling factor λ_D and crack propagation speed. The value of the normalized fields intensity factors may increase or decrease as the applied electric field loading changes from negative to positive, depending on the location of the crack tip. The ‘‘negative’’ means that the direction of the electric loading is opposite to the poling direction. Generally, K_I and K_{II} for the right crack tip increase with increasing the crack

propagation speed and increase with increasing λ_D (Figs. 4(b), 4(c)). The exception being the variation of K_I for large values of propagation speed when the crack speed approaches specific values, which K_I seems to decrease with increasing V/c (Fig. 4(b)). When the crack speed is low, the effects of λ_D upon the mode II stress intensity factor are insignificant. The normalized EDIFs versus the normalized crack speed V/c is depicted in Fig. 4(d). As can be seen, the EDIFs is only weakly dependent on the crack speed, which is a consequence of the quasi-static assumption of the electrical fields. Sghr ogdmnl dmnmhr nardqudc v hsg sgd F`qbÂa-Sánchez et al. [25] and Bagheri [26].

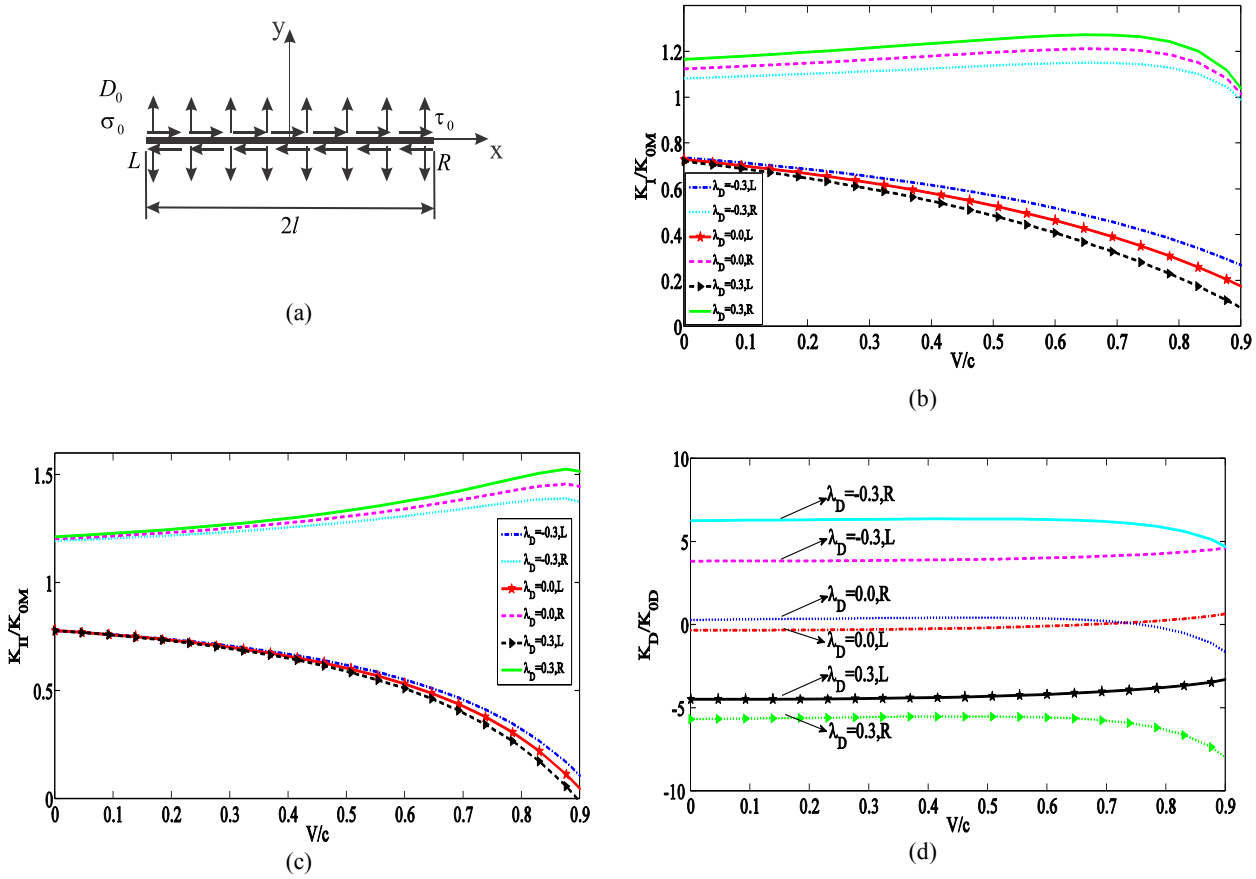

Fig.4
(b) Variation of normalized Mode I SIFs with V/c for different gradient parameter (c) Variation of normalized Mode II SIFs with V/c for different gradient parameter (d) Variation of normalized EDIFs with V/c for different gradient parameter.

4.2 Multiple moving cracks

We consider now the case of FGP plane containing two moving equal-length cracks. The graded material parameter of FGP material is taken as $\beta L = 0.5$. From Fig. 5(b), we observe that the mode I SIFs for the cracks tip, namely R_1 increases with the increase of crack speed for two interacting cracks and the reverse behavior may be observed for crack tips L_1 and L_2. In the case of nonhomogeneous material, due to material asymmetry, the mode I SIFs at L_2 and R_2 are not equal to those at L_1 and R_1. It can be seen that the effect of material gradient becomes stronger than the interaction of the crack tips.

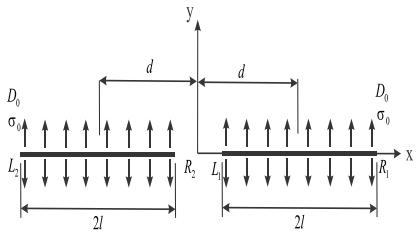

(a)

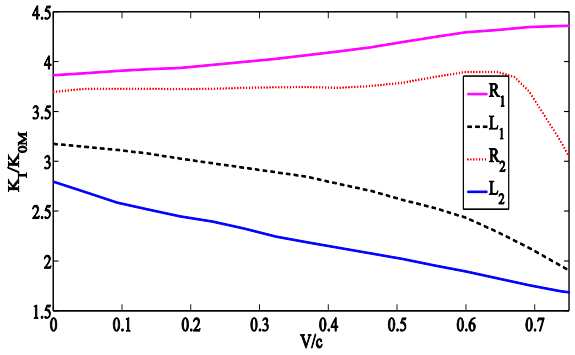

(b)

Fig.5
Variation of normalized Mode I stress intensity factor of two interacting colinear cracks with V/c for $\beta L = 0.5$

In the next example, two moving cracks L_1R_1 and L_2R_2 with equal length $2L = 0.2$ for $\beta L = 0.5$ are considered. The dimensionless modes I and II SIFs are shown in Figs. 6b and 6c. The distance between the crack tips, L_1 and R_2, is minimum. Therefore, the modes I and II for these crack tips have local extreme. In addition, because of very effective interaction of two cracks, SIFs at the crack tips R_2 and L_1 is higher than that at tips L_2 and R_1.

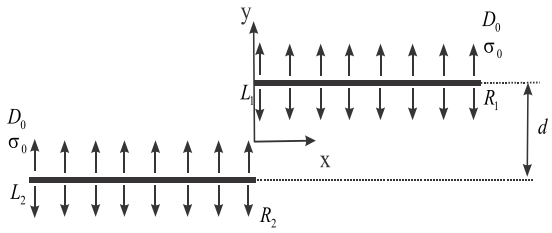

(a)

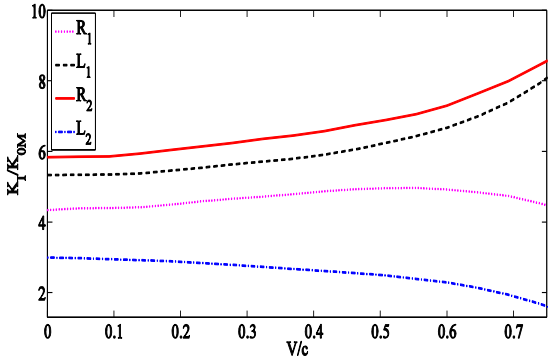

(b)

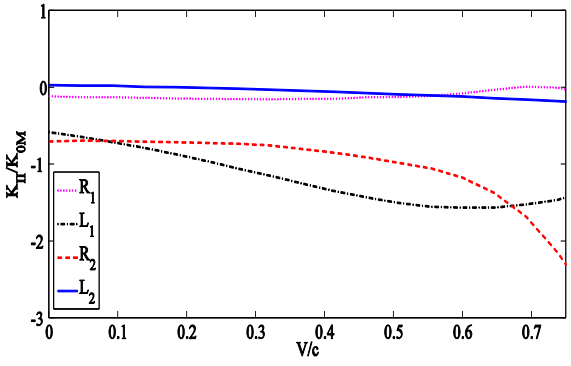

(c)

Fig.6
(b) Variation of normalized Mode I stress intensity factor of two interacting cracks with V/c for $\beta l = 0.5$.(c) Variation of normalized Mode II stress intensity factor of two interacting cracks with V/c for $\beta l = 0.5$.

Figs. 7(b)-7(c) reveal the effect of the crack speed upon the normalized modes I and II SIFs under in-plane loadings for different crack distances for the case where $\beta L = 0.0$. The general feature of these curves is that the mode I SIFs monotonically increase with the increasing of the crack distances up to $V/c = 0.55$. When the distance of the cracks tips is relatively small, the crack tip shielding and anti-shielding effects are observed. The filed

intensity factors increase with the increasing of crack distance in the range between 0.55 and 0.8. Also, the mode I SIFs significantly with the increasing of crack speed when the normalized crack speed approaches the range between 0.55 and 0.8. The mode II SIFs of cracks versus the normalized crack speed V/c are represented in Fig. 7(c). The value of the normalized mode II SIFs may increase or decrease as the crack speed changes, depending on the different crack distance. When the crack speed is high enough, say, $V/c > 0.55$, the variations of Mode II SIFs are significant. The variation of the normalized electric displacement intensity factor with crack speed for different values of crack distance is shown in Fig. 7(d). The trend of variations is the exactly the same as the mode I stress intensity factor.

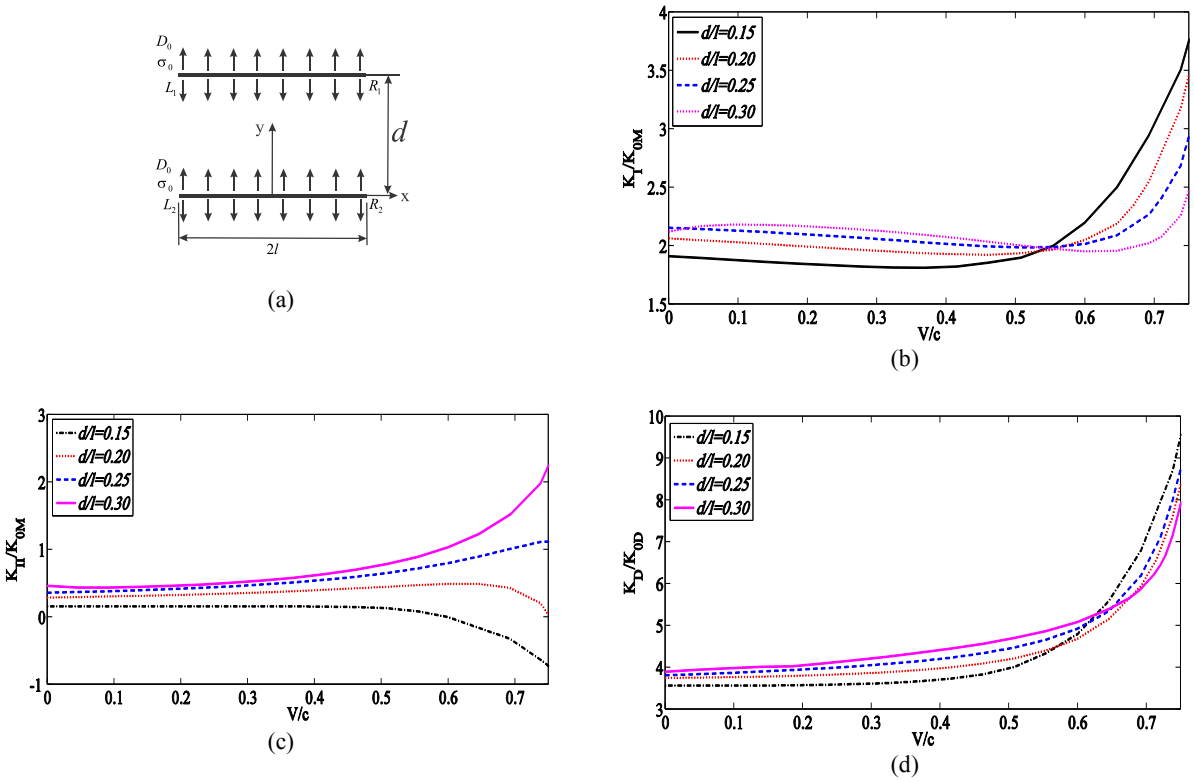

Fig.7
(b) Variation of normalized Mode I stress intensity factor of two interacting parallel cracks with V/c for different crack distances (c) Variation of normalized Mode II stress intensity factor of two interacting parallel cracks (d) Variation of normalized electric displacement intensity factor of two interacting parallel cracks with V/c .

5 CONCLUSION

The solution of dynamic electro-elastic dislocation is obtained in a functionally graded piezoelectric plane. The distributed dislocation technique is used to construct integral equations in the medium weakened by multiple moving cracks under mixed modes condition**.** The numerical solution to integral equations results in the dislocation density function on a crack surface, thereby determining field intensity factors for moving cracks. Numerical results indicate that the crack speed and electric loading have an influence on the dynamic modes I, II and electric displacement intensity factors. It is found that the electric fields may promote or retard crack propagation. On the other hand, the results are highly affected by the graded parameter.

APPENDIX I

The expressions in Eqs. (7) are defined as:

$$\alpha_1=\frac{c_{130}}{c_{440}},\quad \alpha_2=\frac{c_{130}+c_{440}}{c_{440}},\quad \alpha_3=\frac{c_{110}}{c_{440}},\quad \alpha_4=\frac{c_{330}}{c_{440}},\quad \alpha_5=\frac{e_{310}}{c_{440}},\quad \alpha_6=\frac{e_{330}}{c_{440}},\quad \alpha_7=\frac{e_{150}}{c_{440}},$$

$$\alpha_8=\frac{\varepsilon_{330}}{c_{440}},\quad \alpha_9=\frac{\varepsilon_{110}}{c_{440}},\quad c=\sqrt{\frac{c_{440}}{\rho_0}},\quad k=\frac{V}{c}$$

APPENDIX II

The expressions appeared in Eqs. (9) and (12) are:

$$r_1=-\alpha_8$$

$$r_2=(\zeta^2-i\beta\zeta)\alpha_5{}^2-(\beta^2+2i\beta\zeta-2\zeta^2)\alpha_5\alpha_7+[(-i\beta+\zeta)(\alpha_7{}^2+\alpha_3\alpha_8+\alpha_9)-\alpha_8k^2\zeta]\zeta$$

$$r_3=\alpha_9\zeta^2(\zeta-i\beta)[k^2\zeta+i(\beta+i\zeta)\alpha_3],\ r_4=\alpha_5\alpha_6(\beta+i\zeta)+\alpha_1\alpha_8\beta+i\zeta(\alpha_6\alpha_7+\alpha_2\alpha_8)$$

$$r_5=(i\beta\zeta-\zeta^2)[\alpha_5\alpha_7(\beta+i\zeta)+\alpha_1\alpha_9\beta+i\zeta(\alpha_7{}^2+\alpha_2\alpha_9)]$$

$$H_1=(k^2-\alpha_3)\zeta^2+i\beta\zeta\alpha_3,\ H_2=i\zeta\alpha_2+\beta\alpha_1,\ H_3=i\zeta(\alpha_5+\alpha_7)+\beta\alpha_5,\ H_4=i\zeta\alpha_2+\beta$$

$$H_5=(k^2-1)\zeta^2+i\beta\zeta,\ H_6=\alpha_7(i\beta\zeta-\zeta^2),\ H_7=i\zeta(\alpha_5+\alpha_7)+\beta\alpha_7,\ H_8=\alpha_9(-i\beta\zeta+\zeta^2)$$

The functions $A_{ij}, i, j\in\{1,2,3\}$ in Eq. (16) are as follows:

$$A_{11}=\frac{i\zeta\lambda_2(m_2p_1+n_2p_2)-i\zeta\lambda_3(m_3p_1+n_3p_2)+(m_3n_2-m_2n_3)p_3\lambda_2\lambda_3}{p_3[(m_2n_1-m_1n_2)\lambda_1\lambda_2+n_3\lambda_3(m_1\lambda_1-m_2\lambda_2)+m_3\lambda_3(n_2\lambda_2-n_1\lambda_1)]}$$

$$A_{12}=\frac{-i\zeta m_3n_2+i\zeta m_2n_3+n_3\lambda_2-n_2\lambda_3}{m_1(n_3\lambda_2-n_2\lambda_3)+m_2(n_1\lambda_3-n_3\lambda_1)+m_3(n_2\lambda_1-n_1\lambda_2)}$$

$$A_{13}=\frac{-i\zeta m_3n_2\alpha_7+i\zeta m_2n_3\alpha_7+m_2\lambda_3-m_3\lambda_2}{m_1(n_3\lambda_2-n_2\lambda_3)+m_2(n_1\lambda_3-n_3\lambda_1)+m_3(n_2\lambda_1-n_1\lambda_2)}$$

$$A_{21}=-\frac{i\zeta\lambda_1(m_1p_1+n_1p_2)-i\zeta\lambda_3(m_3p_1+n_3p_2)+(m_3n_1-m_1n_3)p_3\lambda_1\lambda_3}{p_3[(m_2n_1-m_1n_2)\lambda_1\lambda_2+n_3\lambda_3(m_1\lambda_1-m_2\lambda_2)+m_3\lambda_3(n_2\lambda_2-n_1\lambda_1)]}$$

$$A_{22}=\frac{i\zeta m_3n_1-i\zeta m_1n_3-n_3\lambda_1+n_1\lambda_3}{m_1(n_3\lambda_2-n_2\lambda_3)+m_2(n_1\lambda_3-n_3\lambda_1)+m_3(n_2\lambda_1-n_1\lambda_2)}$$

$$A_{23}=\frac{i\zeta m_3n_1\alpha_7-i\zeta m_1n_3\alpha_7+m_3\lambda_1-m_1\lambda_3}{m_1(n_3\lambda_2-n_2\lambda_3)+m_2(n_1\lambda_3-n_3\lambda_1)+m_3(n_2\lambda_1-n_1\lambda_2)}$$

$$A_{31}=\frac{i\zeta\lambda_1(m_1p_1+n_1p_2)-i\zeta\lambda_2(m_2p_1+n_2p_2)+(m_2n_1-m_1n_2)p_3\lambda_1\lambda_2}{p_3[(m_2n_1-m_1n_2)\lambda_1\lambda_2+n_3\lambda_3(m_1\lambda_1-m_2\lambda_2)+m_3\lambda_3(n_2\lambda_2-n_1\lambda_1)]}$$

$$A_{32}=\frac{-i\zeta m_2n_1+i\zeta m_1n_2+n_2\lambda_1-n_1\lambda_2}{m_1(n_3\lambda_2-n_2\lambda_3)+m_2(n_1\lambda_3-n_3\lambda_1)+m_3(n_2\lambda_1-n_1\lambda_2)}$$

$$A_{33}=\frac{-i\zeta m_2n_1\alpha_7+i\zeta m_1n_2\alpha_7-m_2\lambda_1+m_1\lambda_2}{m_1(n_3\lambda_2-n_2\lambda_3)+m_2(n_1\lambda_3-n_3\lambda_1)+m_3(n_2\lambda_1-n_1\lambda_2)}$$

where

$$p_1=\alpha_4\alpha_5-\alpha_1\alpha_6,\ p_2=\alpha_5\alpha_6+\alpha_1\alpha_8,\ p_3=\alpha_6{}^2+\alpha_4\alpha_8$$

The integrands are appeared in Eqs. (17) are

$$f_{xx}(x,y,\zeta)=-\frac{ie^{\beta X}c_{440}}{4\pi}\frac{1}{\zeta}[b_x\sum_{j=1}^{3}b_{1j}A_{j1}e^{\lambda_j y}+b_y\sum_{j=1}^{3}b_{1j}A_{j2}e^{\lambda_j y}+b_\varphi\sum_{j=1}^{3}b_{1j}A_{j3}e^{\lambda_j y}]e^{i\zeta x}$$

$$f_{yy}(x,y,\zeta)=-\frac{ie^{\beta X}c_{440}}{4\pi}\frac{1}{\zeta}[b_x\sum_{j=1}^{3}b_{2j}A_{j1}e^{\lambda_j y}+b_y\sum_{j=1}^{3}b_{2j}A_{j2}e^{\lambda_j y}+b_\varphi\sum_{j=1}^{3}b_{2j}A_{j3}e^{\lambda_j y}]e^{i\zeta x}$$

$$f_{xy}(x,y,\zeta)=-\frac{ie^{\beta X}c_{440}}{4\pi}\frac{1}{\zeta}[b_x\sum_{j=1}^{3}b_{3j}A_{j1}e^{\lambda_j y}+b_y\sum_{j=1}^{3}b_{3j}A_{j2}e^{\lambda_j y}+b_\varphi\sum_{j=1}^{3}b_{3j}A_{j3}e^{\lambda_j y}]e^{i\zeta x}$$

$$f_{dx}(x,y,\zeta)=-\frac{ie^{\beta X}c_{440}}{4\pi}\frac{1}{\zeta}[b_x\sum_{j=1}^{3}b_{4j}A_{j1}e^{\lambda_j y}+b_y\sum_{j=1}^{3}b_{4j}A_{j2}e^{\lambda_j y}+b_\varphi\sum_{j=1}^{3}b_{4j}A_{j3}e^{\lambda_j y}]e^{i\zeta x}$$

$$f_{dy}(x,y,\zeta)=-\frac{ie^{\beta X}c_{440}}{4\pi}\frac{1}{\zeta}[b_x\sum_{j=1}^{3}b_{5j}A_{j1}e^{\lambda_j y}+b_y\sum_{j=1}^{3}b_{5j}A_{j2}e^{\lambda_j y}+b_\varphi\sum_{j=1}^{3}b_{5j}A_{j3}e^{\lambda_j y}]e^{i\zeta x}$$

APPENDIX III

The singular part of the integral appeared in Eqs. (19) are:

$$\int_{-\infty}^{\infty}f_{xx\infty}d\zeta=\frac{e^{\beta X}c_{440}}{4\pi}\int_{-\infty}^{\infty}(b_x\sum_{j=1}^{3}\gamma_j\eta_j e^{-\lambda_{jj}|\zeta|y}+i\ \mathrm{sgn}(\zeta)[b_y\sum_{j=1}^{3}\gamma_{j+3}\eta_j e^{-\lambda_{jj}|\zeta|y}+b_\varphi\sum_{j=1}^{3}\gamma_{j+6}\eta_j e^{-\lambda_{jj}|\zeta|y}])e^{i\zeta x}d\zeta$$

$$\int_{-\infty}^{\infty}f_{yy\infty}d\zeta=\frac{e^{\beta X}c_{440}}{4\pi}\int_{-\infty}^{\infty}(b_x\sum_{j=1}^{3}\gamma_j\eta_{j+3}e^{-\lambda_{jj}|\zeta|y}+i\ \mathrm{sgn}(\zeta)[b_y\sum_{j=1}^{3}\gamma_{j+3}\eta_{j+3}e^{-\lambda_{jj}|\zeta|y}+b_\varphi\sum_{j=1}^{3}\gamma_{j+6}\eta_{j+3}e^{-\lambda_{jj}|\zeta|y}])e^{i\zeta x}d\zeta$$

$$\int_{-\infty}^{\infty}f_{xy\infty}d\zeta=\frac{e^{\beta X}c_{440}}{4\pi}\int_{-\infty}^{\infty}(i\ \mathrm{sgn}(\zeta)b_x\sum_{j=1}^{3}\gamma_j\eta_{j+6}e^{-\lambda_{jj}|\zeta|y}-b_y\sum_{j=1}^{3}\gamma_{j+3}\eta_{j+6}e^{-\lambda_{jj}|\zeta|y}-b_\varphi\sum_{j=1}^{3}\gamma_{j+6}\eta_{j+6}e^{-\lambda_{jj}|\zeta|y})e^{i\zeta x}d\zeta$$

$$\int_{-\infty}^{\infty}f_{dx\infty}d\zeta=\frac{e^{\beta X}c_{440}}{4\pi}\int_{-\infty}^{\infty}(i\ \mathrm{sgn}(\zeta)b_x\sum_{j=1}^{3}\gamma_j\eta_{j+9}e^{-\lambda_{jj}|\zeta|y}-b_y\sum_{j=1}^{3}\gamma_{j+3}\eta_{j+9}e^{-\lambda_{jj}|\zeta|y}-b_\varphi\sum_{j=1}^{3}\gamma_{j+6}\eta_{j+9}e^{-\lambda_{jj}|\zeta|y})e^{i\zeta x}d\zeta$$

$$\int_{-\infty}^{\infty}f_{dy\infty}d\zeta=\frac{e^{\beta X}c_{440}}{4\pi}\int_{-\infty}^{\infty}(b_x\sum_{j=1}^{3}\gamma_j\eta_{j+12}e^{-\lambda_{jj}|\zeta|y}+i\ \mathrm{sgn}(\zeta)[b_y\sum_{j=1}^{3}\gamma_{j+3}\eta_{j+12}e^{-\lambda_{jj}|\zeta|y}+b_\varphi\sum_{j=1}^{3}\gamma_{j+6}\eta_{j+12}e^{-\lambda_{jj}|\zeta|y}])e^{i\zeta x}d\zeta$$

where

$$\gamma_1=\frac{(p_1m_{22}+p_2n_{22})\lambda_{22}-(p_1m_{33}+p_2n_{33})\lambda_{33}+(m_{22}n_{33}-m_{33}n_{22})p_3\lambda_{22}\lambda_{33}}{p_3[\lambda_{11}\lambda_{22}(m_{11}n_{22}-m_{22}n_{11})+\lambda_{11}\lambda_{33}(m_{33}n_{11}-m_{11}n_{33})+\lambda_{22}\lambda_{33}(m_{22}n_{33}-m_{33}n_{22})]}$$

$$\gamma_2=\frac{-(p_1m_{11}+p_2n_{11})\lambda_{11}+(p_1m_{33}+p_2n_{33})\lambda_{33}+(m_{33}n_{11}-m_{11}n_{33})p_3\lambda_{11}\lambda_{33}}{p_3[\lambda_{11}\lambda_{22}(m_{11}n_{22}-m_{22}n_{11})+\lambda_{11}\lambda_{33}(m_{33}n_{11}-m_{11}n_{33})+\lambda_{22}\lambda_{33}(m_{22}n_{33}-m_{33}n_{22})]}$$

$$\gamma_3=\frac{(p_1m_{11}+p_2n_{11})\lambda_{11}-(p_1m_{22}+p_2n_{22})\lambda_{22}+(m_{11}n_{22}-m_{22}n_{11})p_3\lambda_{11}\lambda_{22}}{p_3[\lambda_{11}\lambda_{22}(m_{11}n_{22}-m_{22}n_{11})+\lambda_{11}\lambda_{33}(m_{33}n_{11}-m_{11}n_{33})+\lambda_{22}\lambda_{33}(m_{22}n_{33}-m_{33}n_{22})]}$$

$$\gamma_4=\frac{(m_{33}n_{22}-m_{22}n_{33}-n_{33}\lambda_{22}+n_{22}\lambda_{33})}{m_{33}(\lambda_{11}n_{22}-\lambda_{22}n_{11})+m_{22}(\lambda_{33}n_{11}-\lambda_{11}n_{33})+m_{11}(\lambda_{22}n_{33}-\lambda_{33}n_{22})}$$

$$\gamma_5=\frac{(m_{11}n_{33}-m_{33}n_{11}-n_{11}\lambda_{33}+n_{33}\lambda_{11})}{m_{33}(\lambda_{11}n_{22}-\lambda_{22}n_{11})+m_{22}(\lambda_{33}n_{11}-\lambda_{11}n_{33})+m_{11}(\lambda_{22}n_{33}-\lambda_{33}n_{22})}$$

$$\gamma_6=\frac{(m_{22}n_{11}-m_{11}n_{22}-n_{22}\lambda_{11}+n_{11}\lambda_{22})}{m_{33}(\lambda_{11}n_{22}-\lambda_{22}n_{11})+m_{22}(\lambda_{33}n_{11}-\lambda_{11}n_{33})+m_{11}(\lambda_{22}n_{33}-\lambda_{33}n_{22})}$$

$$\gamma_7=\frac{(m_{33}n_{22}\alpha_7-m_{22}n_{33}\alpha_7-m_{22}\lambda_{33}+m_{33}\lambda_{22})}{m_{33}(\lambda_{11}n_{22}-\lambda_{22}n_{11})+m_{22}(\lambda_{33}n_{11}-\lambda_{11}n_{33})+m_{11}(\lambda_{22}n_{33}-\lambda_{33}n_{22})}$$

$$\gamma_8=\frac{(m_{11}n_{33}\alpha_7-m_{33}n_{11}\alpha_7-m_{33}\lambda_{11}+m_{11}\lambda_{33})}{m_{33}(\lambda_{11}n_{22}-\lambda_{22}n_{11})+m_{22}(\lambda_{33}n_{11}-\lambda_{11}n_{33})+m_{11}(\lambda_{22}n_{33}-\lambda_{33}n_{22})}$$

$$\gamma_9=\frac{(m_{22}n_{11}\alpha_7-m_{11}n_{22}\alpha_7-m_{11}\lambda_{22}+m_{22}\lambda_{11})}{m_{33}(\lambda_{11}n_{22}-\lambda_{22}n_{11})+m_{22}(\lambda_{33}n_{11}-\lambda_{11}n_{33})+m_{11}(\lambda_{22}n_{33}-\lambda_{33}n_{22})}$$

$\eta_j=\alpha_3-\alpha_1 m_{jj}\lambda_{jj}-\alpha_5 n_{jj}\lambda_{jj}$, $\eta_{j+3}=\alpha_1-\alpha_4 m_{jj}\lambda_{jj}-\alpha_6 n_{jj}\lambda_{jj}$, $\eta_{j+6}=\lambda_{jj}+m_{jj}+\alpha_7 n_{jj}$,

$\eta_{j+9}=\alpha_7\lambda_{jj}+\alpha_7 m_{jj}-\alpha_9 n_{jj}$, $\eta_{j+12}=\alpha_5-\alpha_6 m_{jj}\lambda_{jj}+\alpha_8 n_{jj}\lambda_{jj}$, $j=1,2,3$

$$m_{jj}=\frac{-\alpha_8\lambda_{jj}^{\ 4}+(\alpha_5^{\ 2}+2\alpha_5\alpha_7+\alpha_7^{\ 2}-k^2\alpha_8+\alpha_3\alpha_8+\alpha_9)\lambda_{jj}^{\ 2}+(k^2\alpha_9-\alpha_3\alpha_9)}{(\alpha_5\alpha_6+\alpha_6\alpha_7+\alpha_2\alpha_8)\lambda_{jj}^{\ 3}-(\alpha_5\alpha_7+\alpha_7^{\ 2}+\alpha_2\alpha_9)\lambda_{jj}},\quad j=1,2,3$$

$$n_{jj}=\frac{-\lambda_{jj}^{\ 2}-\alpha_2 m_{jj}\lambda_{jj}+(\alpha_3-k^2)}{(\alpha_5+\alpha_7)\lambda_{jj}},\quad j=1,2,3$$

$$\lambda_{11}=\sqrt{\frac{\Delta_{11}}{3}+\frac{2^{1/3}p_{11}}{3(q_{11}+r_{11})^{1/3}}+\frac{(q_{11}+r_{11})^{1/3}}{3\times 2^{1/3}}}$$

$$\lambda_{22}=\sqrt{\frac{\Delta_{11}}{3}-\frac{(1+i\sqrt{3})p_{11}}{3\times 2^{2/3}(q_{11}+r_{11})^{1/3}}+\frac{(-1+i\sqrt{3})(q_{11}+r_{11})^{1/3}}{6\times 2^{1/3}}}$$

$$\lambda_{33}=\sqrt{\frac{\Delta_{11}}{3}-\frac{(1-i\sqrt{3})p_{11}}{3\times 2^{2/3}(q_{11}+r_{11})^{1/3}}-\frac{(1+i\sqrt{3})(q_{11}+r_{11})^{1/3}}{6\times 2^{1/3}}}$$

$$\Delta_{11}=\frac{\alpha_4\alpha_9+\alpha_6(2\alpha_7-2\alpha_2(\alpha_5+\alpha_7)+(\alpha_3-k^2)\alpha_6)+\alpha_4(\alpha_5+\alpha_7)^2+\alpha_8(\alpha_4(\alpha_3-k^2)-\alpha_2^{\ 2}+(1-k^2))}{\alpha_4\alpha_8+\alpha_6^{\ 2}}$$

$$\Delta_{22}=\frac{\alpha_7^{\ 2}+(1-k^2)[(\alpha_5+\alpha_7)^2+\alpha_9+\alpha_8(\alpha_3-k^2)]-2\alpha_2\alpha_7(\alpha_5+\alpha_7)-\alpha_2^{\ 2}\alpha_9+(\alpha_3-k^2)[\alpha_4\alpha_9+2\alpha_6\alpha_7]}{\alpha_4\alpha_8+\alpha_6^{\ 2}}$$

$$\Delta_{33}=\frac{(\alpha_3-k^2)[\alpha_7^{\ 2}+(1-k^2)\alpha_9]}{\alpha_4\alpha_8+\alpha_6^{\ 2}}$$

$p_{11}=\Delta_{11}^{\ 2}-3\Delta_{22}$, $q_{11}=2\Delta_{11}^{\ 3}-9\Delta_{11}\Delta_{22}+27\Delta_{33}$, $r_{11}=\sqrt{-4p_{11}^{\ 3}+q_{11}^{\ 2}}$.

REFERENCES

[1] Ikeda T., 1996, *Fundamentals of Piezoelectricit*, Oxford University Press.

[2] Cheng Zh., Suia Zh., Yin H., Fenga, H., 2019, Numerical simulation of dynamic fracture in functionally graded materials using peridynamic modeling with composite weighted bonds, *Engineering Analysis with Boundary Elements* **105**: 31-46.

[3] Hassanifard S., Mohtadi Bonab M.A., Jabbari Gh., 2013, Investigation of fatigue crack propagation in spot-welded joints based on fracture mechanics approach, *Journal of Materials Engineering and Performance* **22**: 245-250.

[4] Mohtadi Bonab M.A., Eskandari M., Szpunar J.A., 2016, Effect of arisen dislocation density and texture components

during cold rolling and annealing treatments on hydrogen induced cracking susceptibility in pipeline steel, *Journal of Materials Research* **31**: 3390-3400.

[5] Kwon J.H., Lee K.Y., Kwon S.M., 2000, Moving crack in a piezoelectric ceramic strip under anti-plane shear loading, *Mechanics Research Communications* **27**: 327-332.

[6] Gao C.F., Zhao Y.T., Wang M.Z., 2001, Moving antiplane crack between two dissimilar piezoelectric media, *International Journal of Solids and Structures* **38**: 9331-9345.

[7] Li B.C., Weng G.J., 2002, Yoffe-type moving crack in a functionally graded piezoelectric material, *Proceedings of the Royal Society of London* **458**: 381-399.

[8] Megiud S.A., Wang X.D., Jiang L.Y., 2002, On the dynamic propagation of a finite crack in functionally graded materials, *Engineering Fracture Mechanics* **69**: 1753-1768.

[9] Wang X., Zhong Z., Wu F.L., 2003, A moving conducting crack at the interface of two dissimilar piezoelectric materials, *International Journal of Solids and Structures* **40**: 2381-2399.

[10] Li X.F., 2003, Griffith crack moving in a piezoelectric strip, *Archive of Applied Mechanics* **72**: 745-758.

[11] Hu K., Zhong Z., 2006, A moving mode-III crack in a functionally graded piezoelectric strip, *International Journal of Mechanics and Materials in Design* **2**: 61-79.

[12] Piva A., Tornabene F., Viola E., 2007, Subsonic Griffith crack propagation in piezoelectric media, *European Journal of Mechanics-A/Solids* **26**: 442-459.

[13] Yan Z., Jiang L.Y., 2009, Study of a propagating finite crack in functionally graded piezoelectric materials considering dielectric medium effect, *International Journal of Solids and Structures* **46**: 1362-1372.

[14] Lapusta Y., Komarov A., Labesse-Jied F., MoutouPitti R., Loboda V., 2011, Limited permeable crack moving along the interface of a piezoelectric bi-material, *European Journal of Mechanics-A/Solids* **30**: 639-649.

[15] Li Y.D., Lee K.Y., 2010, Two collinear unequal cracks in a poled piezoelectric plane: Mode I case solved by a new approach of real fundamental solutions, *International Journal of Fracture* **165**: 47-60.

[16] Asadi E., 2011, Analysis of multiple axisymmetric annular cracks in a piezoelectric medium, *European Journal of Mechanics-A/Solids* **30**: 844-853.

[17] Bagheri R., Ayatollahi M., Mousavi S.M., 2015, Stress analysis of a functionally graded magneto-electro-elastic strip with multiple moving cracks, *Mathematics and Mechanics of Solids* **22**: 304-323.

[18] Bagheri R., Ayatollahi M., Mousavi S.M., 2015, Analysis of cracked piezoelectric layer with imperfect non-Homogeneous orthotropic coating, *International Journal of Mechanical Sciences* **93**: 93-101.

[19] Monfared M.M., Ayatollahi M., Bagheri R., 2016, In-plane stress analysis of dissimilar materials with multiple interface cracks, *Applied Mathematical Modelling* **40**: 8464-8474.

[20] Wang X., Pan E., 2008, Three-dimensional quasi-steady-state problem of moving heat and diffusion sources in an infinite solid, *Mechanics Research Communications* **35**: 475-482.

[21] Monfared M.M., Ayatollahi M., 2017, Interactions of multiple cracks in a transversely isotropic piezoelectric plane under mixed mode condition, *Engineering Fracture Mechanics* **180**: 87-104.

[22] Bagheri R., 2017, Several horizontal cracks in a piezoelectric half-plane under transient loading, *Archive of Applied Mechanics* **87**: 1979-1992.

[23] Delale F., Erdogan F., 1983, The crack problem for a nonhomogeneous plane, *Journal of Applied Mechanics* **50**: 609-614.

[24] Bagheri R., Noroozi M., 2018, The linear steady state analysis of multiple moving cracks in a piezoelectric half-plane under in-plane electro-elastic loading, *Theoretical and Applied Fracture Mechanics* **96**: 334-350.

[25] García-Sánchez F., Zhang Ch., Sládek J., Sládek V., 2007, 2D transient dynamic crack analysis in piezoelectric solids by BEM, *Computational Materials Science* **39**: 179-186.

[26] Bagheri R., 2017, Several horizontal cracks in a piezoelectric half-plane under transient loading, *Archive of Applied Mechanics* **87**: 1979-1992.